EasyChair Preprint

№ 3028

Extraction of Dual-Band Antenna Response from UWB Based on Current Distribution Analysis

Mahmood Yassen, Jawad Ali, Mohammed Hussan, Ali Salim and Hussam Alsaedi

March 22, 2020

Extraction of Dual-Band Antenna Response from UWB Based on Current Distribution Analysis

Mahmood T. Yassen, Jawad K. Ali, Mohammed R. Hussan, Ali J. Salim, and Hussam Alsaedi
Microwave Research Group, Department of Electrical Engineering, University of Technology, Iraq
E-mail: jawengin@yahoo.com

ABSTRACT

In this paper, a new design technique of printed dual-band monopole antenna has been introduced. The design proposed is significantly based on the ultra-wideband (UWB) printed monopole antenna structure. The presented antennas have been modeled using a substrate having 1.6 mm thickness and a relative dielectric constant of 4.6 and have been fed with a 50 Ohm coplanar waveguide (CPW) transmission line. Modeling and performance evaluation of the antennas, presented in this paper, have been carried out using the commercially available Computer Simulation Technique (CST) EM simulator. Furthermore, it has been found that applying the fractal geometry on the radiating element, results in an enhanced resonance of the dual-band antenna and a better coupling of the obtained resonating bands.

Keywords: Multiband antenna, UWB antenna, Microstrip antenna, Fractal geometry.

1. INTRODUCTION

The increasing range of wireless communication services and related applications are drawing the attention of the design of dual-band and small antennas. The telecom operators and equipment manufacturers can produce a variety of communication systems, like cellular communications, global positioning, satellite communications, and others. Each of these systems operates in several frequency bands. Each system needs to have an antenna that has to work in the frequency band employed for the particular system to serve the users. In the past, the tendency had used one antenna for each system, but this solution is inefficient regarding space usage, and it is an expensive one. The variety of communication systems suggests that there is a need for dual-band or multiband antennas. There are quite a few techniques currently available to achieve dual-band operation with printed and microstrip antennas. We can divide these techniques into three design categories.

The first category is a single patch design; this design category is considered the most straightforward and is widely used in the field of dual-band microstrip antennas. Single patch design can be subdivided into two types; the first type involves the use of the first resonance of the two orthogonal dimensions of the rectangular patch [1]. In this case, the frequency ratio is approximately equal to the ratio of the two orthogonal sides of the patch. The apparent limitation of this approach is that the two different frequencies excite two orthogonal polarizations. However, this simple method is beneficial in low–cost short–range applications where polarization requirements are not pressing.

The second type of design is to introduce a reactive loading to a single patch, including capacitors or varactors [2, 3], notches [4], pin diode [5], stubs [6, 7]. And slots are also used, which are either external slots [8-12] or embedded slots [13-15]. By these reactive-loading approaches, one can modify the resonant mode of the patch, so that the radiation pattern of the higher-order mode could be similar to that of the fundamental mode.

The dual-band operation can also be achieved using two or more radiating elements on the same substrate, each of them supporting high currents and radiation at the resonance as the second design category [16-18]. This category also includes multi-layer stacked patches on a multi-substrate that can use patches of various shapes [16]. These antennas operate with the same polarization at the two frequencies, as well as with dual polarization. The same multilayer structures can also be used to broaden the bandwidth of a single band antenna when the two frequencies are forced to be closely-spaced.

The third category involves the use of fractal geometry in the design of dual-band antennas. In this context, the unique properties of the various fractal geometries have been successfully applied to design compact size antennas and other microwave circuits and components. Different fractal structures have been used in the design of numerous miniaturized types of filters for many applications adopting the space-filling property [19-32].

However, this property could support the design of compact dual-band and multiband when combined with other techniques [33-40]. In this case, approaches such as the stepped-impedance resonator, SIR, have been successfully adopted to achieve such a task. Besides, using multiple structures, such that each resonator resonates at its resonant frequency, has been widely used.

The properties of fractal geometry permit the dual-band behavior to be achieved with fractal shaped antenna structures. Space-filling [41-42] property of fractal geometry could be used for miniaturizing antenna size and also for improving the response of the dual-band antenna. Their property of being self-similarity in the geometry leads to having dual-band [43-45], and multiband [46-47] antennas which have a large number of non-harmonic resonant frequencies. Fractal antennas have

improved impedance and voltage standing wave ratio (VSWR) performance on a reduced physical area when compared to non-fractal Euclidean geometries.

In this paper, a new design technique for the printed dual-band antenna is proposed. In this technique, the dual-band resonant behavior is to be extracted from the UWB response. The current distributions on the surface of the UWB antenna have to be investigated at different frequencies to show the contributions of the antenna parts in the resulting resonances. Accordingly, the dual-band resonant behavior can be extracted by modifying the antenna structure to enhance the currents at the required resonant frequencies.

Furthermore, the philosophy of the proposed technique relies on the fact that the resonant behavior of any UWB antenna is composed of a vast number of resonant bands coupled together to form the resulting response. These resonant bands have been attributed to the different parts of the antenna structure. This can be monitored by examining the current distributions on the surface of the antenna structure at these bands. The dual-band behavior of the antenna can be derived from UWB one through the modifications on the different parts of the antenna structure with the aid of the related current distribution.

2. THE SQUARE PRINTED MONOPOLE UWB ANTENNA

Since the U.S. Federal Communications Commission (FCC) announced the use of the ultra-wideband (UWB) range, i.e., 3.1-10.6 GHz for commercial purposes, academic and industrial researches become dramatically increased in this technology. Two crucial techniques for antenna engineering design are bandwidth enhancement along with antenna miniaturization. Recently, many researchers have proposed different methods to design compact size antennas along with wide-bandwidth performance to satisfy the resonance of UWB for several applications.

2.1 The Reference UWB Antenna Structure

The geometry of the proposed square printed monopole UWB antenna is shown in Figure 1. Figure 1 displays the front view of the structure, which contains the radiator, and the coplanar waveguide (CPW) feed technique. The total size of the proposed antenna, including the substrate, is 43 × 40 mm2, which has been supposed to be printed on FR4 glass epoxy substrate of thickness 1.6 mm, and relative permittivity of 4.6.

The radiator is in the form of a square patch having the dimension of (Wp × Lp) and excited using a (50) Ω coplanar waveguide (CPW) feed technique. The dimension of the feed line is (Wf × Lf), and the gap between the feed line and the ground plane is (g1), whereas the gap between the ground plane and the radiator is (g2). Slots are cut from the upper and lower corners of the patch in a stepped manner with the dimensions Wst1 × Lst1, Wst2 × Lst2, and Wst3 × Lst3.

The dimension of the ground plane is (Wgp × Lgp) at both sides of the feed line. The final values of the optimum parameters are indexed in Table 1. It is worth to note that all dimensions are in (mm).

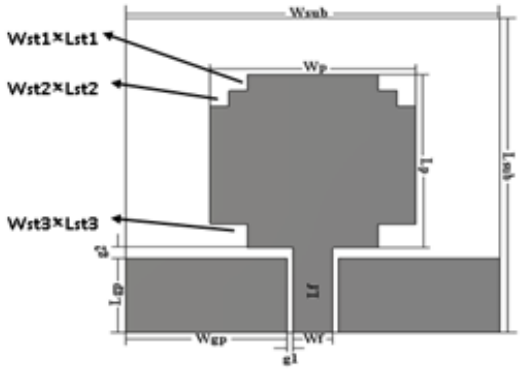

Figure-1. The proposed printed monopole UWB antenna

Table 1: Details of the proposed antenna parameters as labeled in Figure 1

Antenna Components	Symbols and their values of the proposed antenna in (mm)
Radiator	Wp = 22, Lp = 22
Upper Steps	Wst1 = 2, Lst1 = 2, Wst2 = 2, Lst2 = 2
Lower Steps	Wst3 = 4, Lst3 = 3
Feed Line	CPW, Wf = 4.2, Lf = 10.79, g1=0.66, g2=1.29
Ground plane	Wgp = 17.24, Lgp = 9.5
Substrate	Wsub = 40, Lsub = 43, h=1.6

2.2 The Reference UWB Antenna Design

Observing the influence of the various parameters on the antenna performance, it has been found that the dominant factor in the proposed square printed monopole UWB antenna is the patch length (Lp) in terms of the guided wavelength λg.

$$\lambda_g = \frac{\lambda_\circ}{\sqrt{\varepsilon_{reff}}} \quad (1)$$

where ε_{reff} is the effective relative dielectric constant, a value for the effective relative dielectric constant ε_{reff}, with a feed line width, Wf to the substrate height ratio Wf/h ≥ 1, using:

$$\varepsilon_{reff} = \frac{\varepsilon_r + 1}{2} + \frac{\varepsilon_r - 1}{2}\left(\frac{1}{\sqrt{1+12h/W_f}}\right) \quad (2)$$

Then the lower resonant frequency, (fL), relative to the radiating element length (Lp) is determined by:

$$f_L \approx \frac{C_\circ}{2(L_p + \Delta L)\sqrt{\varepsilon_{reff}}} \quad (3)$$

where Co is the speed of light in free space, ΔL is the incremental length which accounts for the fringing of the field at respective edges:

$$\Delta L \approx W_{st1} + W_{st3} \quad (4)$$

2.3 The Performance of the Modeled UWB Antenna

Simulation results of the proposed printed monopole UWB antenna have been shown in Figures 2 and 3. Figure 2 shows the S_{11} response of this antenna with respect to 50 Ω transmissions, in a simulation swept-

frequency range from 1 to 11 GHz. In this frequency range, the proposed antenna exhibits good UWB characteristics with a wide operating range of 2.8 to 10.65 GHz, and the lower resonance frequency 2.8 GHz is determined by the square patch length Lp and governed by the Equation (3). The first, second, third, and fourth pole frequencies are 3.77 GHz, 5.82 GHz, 7.93 GHz, and 9.74 GHz, at which the values of S11 are -37.41 dB, -22.3 dB, -18.3 dB, and -30.94 dB respectively. Due to these pole frequencies, the antenna exhibits an UWB response. As observed from Figure 2, the value of S11 is well below -10 dB throughout the UWB frequency band.

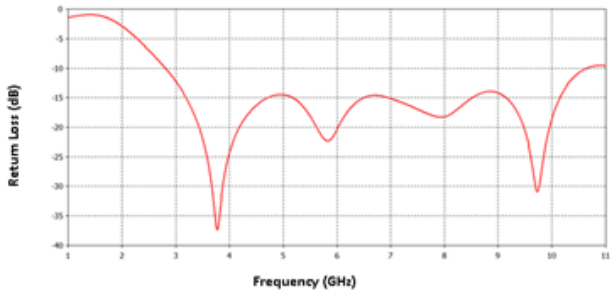

Figure-2. The simulated input reflection coefficient of the proposed printed monopole UWB antenna

The plots of the current distribution of the proposed UWB antenna at different resonance frequencies are shown in Figure 3. Figures 3(a) and 3(b) show the current distribution at the lower resonance frequency 2.8 GHz and the first pole frequency 3.77 GHz; it has been depicted the current concentration at the side lengths of the radiator with the lower steps in the radiation at these frequencies. In Figures 3(c) and (d), it can be seen that the upper steps together with the lower steps and the side lengths of the radiator have direct effects on the radiation of the second and third pole of resonance frequencies 5.82, and 7.93 GHz respectively. At the fourth pole of resonance frequency 9.74 GHz and the upper resonance frequency 10.65 GHz, the strong resonant current is exciting the lower width and the lower steps of the radiator. The current is also concentrated at the upper width of the ground plane and the internal lengths around the feed line with the mainly flowing of it along the feed line. However, it is always flowing along the feed line at all the resonance frequencies.

2.4 The Effects of Steps on the Resonance of the Proposed UWB Antenna

The impedance bandwidth is the essential characteristic of the UWB antenna, and the good UWB antenna should be capable of operating over the bandwidth assigned by the FCC.

Many techniques are used to increase the bandwidth of the UWB antenna, and slots are considered the most popular method for this purpose. In the proposed antenna, slots in the form of a square and rectangular cut are introduced in the upper and lower corners of the patch in a stepped manner as in [48], to provide wideband matching of the transmission system with the radiator.

Figure 4 illustrates the effects of these steps, and it is observed that the insertion of these steps is the most compelling manner for getting the broad bandwidth as well as proper impedance matching to maximize the antenna radiation efficiency.

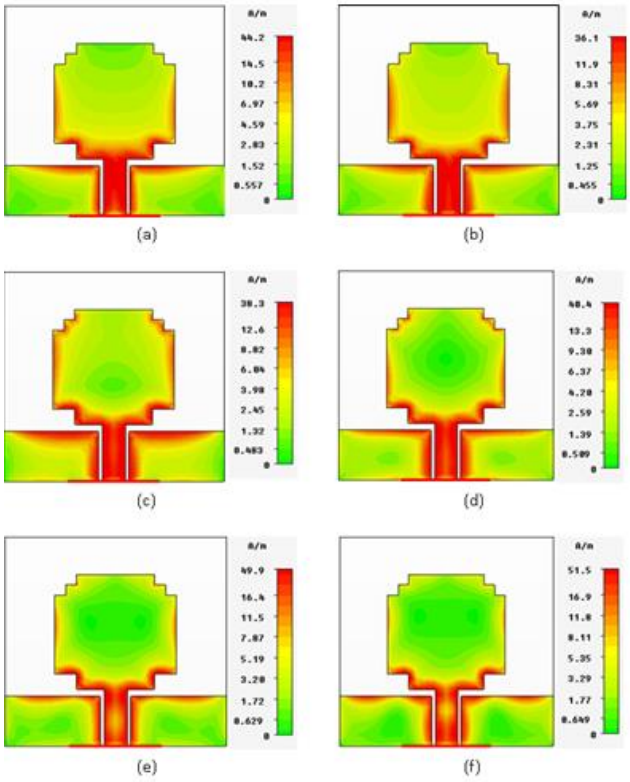

Figure-3. Simulated current distributions on the surface of the proposed UWB antenna at (a) 2.8 GHz, (b) 3.77 GHz, (c) 5.82 GHz, (d) 7.93 GHz, (e) 9.74 GHz, and (f) 10.65 GHz

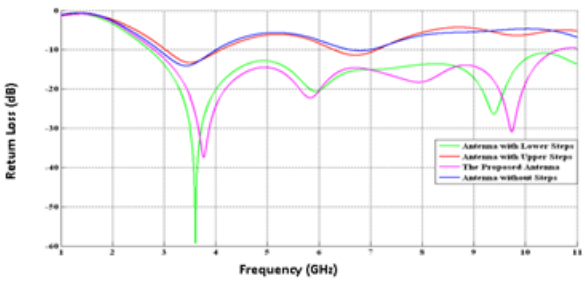

Figure-4. Effects of steps on the resonance of the proposed UWB antenna

3. MODIFICATIONS ON THE UWB ANTENNA ELEMENTS

Based on the surface current distribution and the resonance of the proposed UWB antenna, two primary modifications procedures have contributed to extract dual-band resonance behavior from the obtained UWB resonance in square printed monopole antenna. The first is the patch modification, and the second is the ground plane and feed line modification with the same substrate characteristics and feeding technique used in the proposed UWB antenna. The idea of these modifications is to remove any regions from the patch and ground plane responsible for making resonance in the upper frequencies in UWB resonance. Also, increase the current in the areas responsible for making resonance in the lower frequencies in UWB resonance.

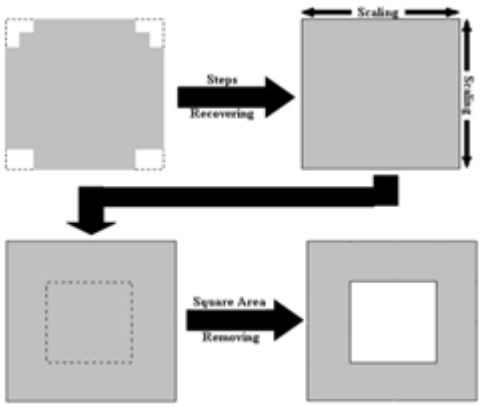

Figure-5. Antenna radiating element modifications

3.1 Modifications on the Antenna Radiating Element

The antenna patch modification can be explained by Figure 5. The first process is the recovery of the steps to remove their effect of broadening the resonance, so Figure 4 shows that there are two bands with S11 ≤ -10 dB after recovering steps. The second process is the increasing of the patch dimensions to minimize the lower resonance frequency. The middle area of the patch has no relation to the lower resonance frequency, as shown in Figure 3. The third process is to remove the square area from the middle of the patch to increase the amount of current in the crucial regions of the lower resonance frequency.

3.2 Modifications on Antenna Ground Plane and Feed Line

Figure 6 simplifies the antenna ground plane and feed line modification. The purpose of the decreasing process in feed line width is to increase the impedance matching for the obtained resonating bands after patch modification, and the use of the ground plane area reduction is to enhance the bandwidth of the high resonance band. As shown in Figure 3(c), a large amount of current concentrated at the upper width of the ground plane and the internal lengths around the feed line. Therefore, the aim of the notch insertion to the ground plane is to increase the total current in this region, and this will increase the resonance frequency generation.

4. THE RESULTING ANTENNA DESIGN

The resulting dual-band antenna by using the modifying processes on the proposed UWB antenna should maintain the reasonable bandwidth, gain, and radiation characteristics to satisfy the wireless communication applications. The tools of the CST software are used to examine the resulting antenna characteristics. The details of the antenna structure, antenna design, and performance evaluation are explained in the following items.

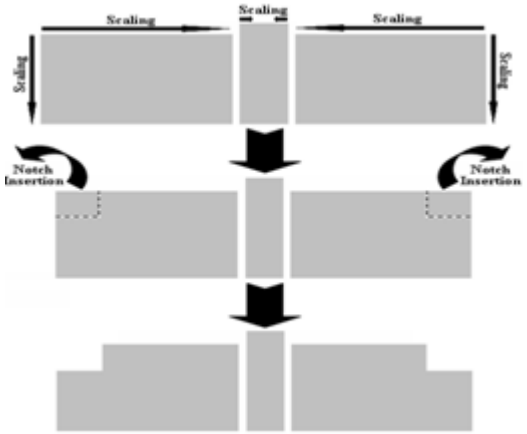

Figure-6. Antenna ground plane and feed line modifications

4.1 The Antenna Structure

The geometry of the resulting dual band antenna as the front view is shown in Figure 7. The radiator is in the form of a square ring having an external dimension (Wp × Lp), and the internal (slot) dimension (Ws × Ls) is excited using the same feed technique of the proposed UWB antenna. Two rectangular slots with a size of (Wno × Lno) have been cut from each upper corner of the ground plane. Table 2 summarizes the modified dimensions of the resulting antenna parameters, as labeled in Figure 7.

Figure-7. The resulting square printed monopole dual-band antenna.

Table 2: Details of the modified parameters of the resulting dual-band antenna, as labeled in Figure 7

Antenna Components	Symbols and their values of the proposed antenna in (mm)
Radiator	Wp = 24, Lp = 24
Inner Square Slot	Ws = 12, Ls = 12
Feed Line	CPW, Wf = 3, Lf = 10.79, g1=0.66, g2=1.59
Ground plane	Wgp = 15.34, Lgp = 9.2
Ground Plane Notch	Wno = 7, Lno = 5
Substrate	Wsub = 40, Lsub = 43, h=1.6

4.2 The Resulting Antenna Design

The resulting square printed monopole dual-band antenna has been designed to serve the wireless communication applications. After modification processes and dimensions scaling, it has been found that the internal slot length (Ls), and about of 77% from the external length (Lp) of the radiator have the direct effect on the resonance of the lower frequency as an effective length (Leff) in terms of the guided wavelength λg. Then the effective length Leff can be formulated by:

$$L_{eff} = L_s + 0.77L_p \quad (5)$$

The lower resonant frequency, (f_{L1}), relative to the length of the radiating element (effective length) is determined by:

$$f_{L1} \approx \frac{C_\circ}{2L_{eff}\sqrt{\varepsilon_{reff}}} \quad (6)$$

where Co is the speed of light in free space.

4.3 The Resulting Antenna Performance

Simulation results of the resulting square printed monopole dual-band antenna have been shown in Figures 8 to 12. Figure 8 shows the input reflection coefficient response of the resulting antenna in a simulation swept frequency range from 1 to 10 GHz.

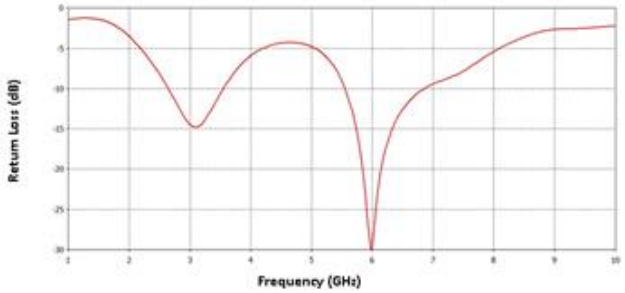

Figure-8. The simulated input reflection coefficient of the resulting square printed monopole dual-band antenna

The dual-band behavior of this antenna is quite clear. In this frequency range, there are two resonating frequency bands (for S11 < -10 dB): the lower resonant band from 2.64 – 3.55 GHz with center frequency of 3.08 GHz for -14.8 dB S11, and the upper resonant band from 5.55 – 6.85 GHz with center frequency of 5.98 GHz for -29.97 dB S11, with corresponding bandwidths of 0.91 and 1.3 GHz respectively. The frequency ratio (f_{o1}/f_o2) of this antenna is 0.52.

The surface current distribution has been studied using the simulation tool and illustrated in Figure 9. Figure 9(a) shows the surface current of the resulting antenna at the center frequency 3.08 GHz of the lower resonant band; the current is concentrated at the internal slot lengths, a part of external lengths, and at the lower width of the radiator.

Figure 9(b) shows the surface current of the resulting antenna at the center frequency of 5.98 GHz of the upper resonant band; the current is concentrated at the two upper internal corners and the lower width of the radiator. The current has mainly flowed along the feed line at both mentioned frequencies.

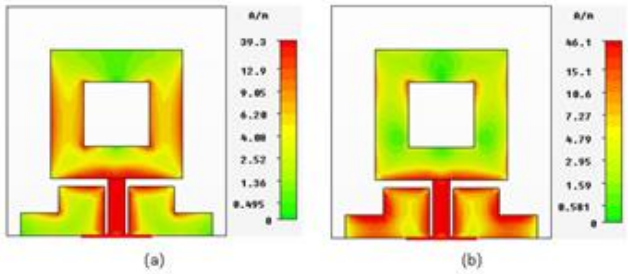

Figure-9. Simulated current distributions on the surface of the resulting square printed monopole dual-band antenna at (a) 3.08 GHz, and (b) 5.98 GHz

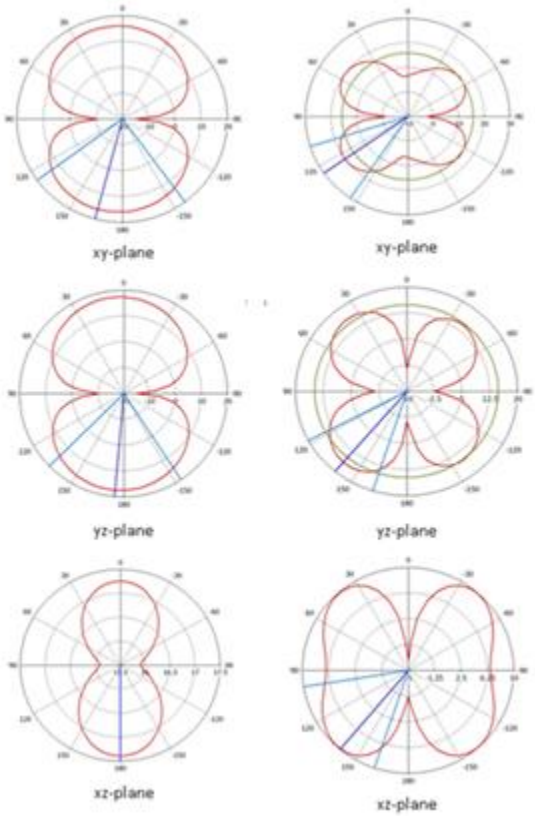

Figure-10. Simulated far-field radiation patterns for the total electric field of the resulting square printed monopole dual-band antenna at (a) 3.08 GHz, and (b) 5.98 GHz

Figure 10 shows the simulated antenna far-field radiation patterns for the total electric field in the x-y plane, the x-z plane, and the y-z plane at the center frequencies of the two bands. Figure 10(a) depicts the radiation patterns at 3.08 GHz. In the x-y plane ($\theta = 90^o$), the main lobe magnitude is 16.1 dB, the main lobe direction is (167^o), and the angular width (3 dB) is (90.4^o). In the x-z plane ($\varphi = 0^o$), the main lobe magnitude is 17.4 dBV/m, and the main lobe direction is (180^o). Whereas in the y-z plane ($\varphi = 90^o$), the main lobe magnitude is 17.5 dBV/m, the main lobe direction is (173^o), and the angular

width (3 dB) is (79°). Figure 10(b) presents the radiation patterns at 5.98 GHz. In the x-y plane (θ = 90°), the main lobe magnitude is 20 dB, the main lobe direction is (126°), the angular width (3 dB) is (38.5°), and the sidelobe level is -4.2 dB. In the x-z plane (φ = 0°), the main lobe magnitude is 10 dB, the main lobe direction is (138°), and the angular width (3 dB) is (62.1°). Whereas in the y-z plane (φ = 90°), the main lobe magnitude is 16.5 dB, the main lobe direction is (142°), the angular width (3 dB) is (44.4°), and the sidelobe level is -1.7 dB.

As far as the radiation properties are concerned, Figure 11 shows the simulated three-dimensional directivity radiation patterns of the resulting antenna. The directivity at 3.08 GHz, the center frequency of the lower band, is 2.66 dBi, as shown in Figure 11(a), whereas the directivity at 5.98 GHz the center frequency of upper band is 5.27 dBi as shown in Figure 11(b).

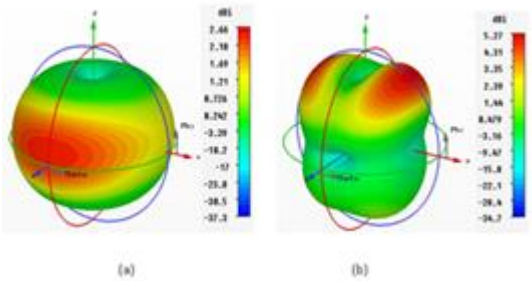

Figure-11. Simulated 3D directivity of the resulting square printed monopole dual-band antenna at (a) 3.08 GHz, and (b) 5.98 GHz

The peak gain values in the two bands have been evaluated, as shown in Figure 12. In the lower frequency band, the peak gain plotted in Figure 12(a) is as large as 1.59 dBi. The gain versus frequency, for the upper band, is plotted in Figure 12(b), where the maximum gain is found to be of about 6.14 dBi.

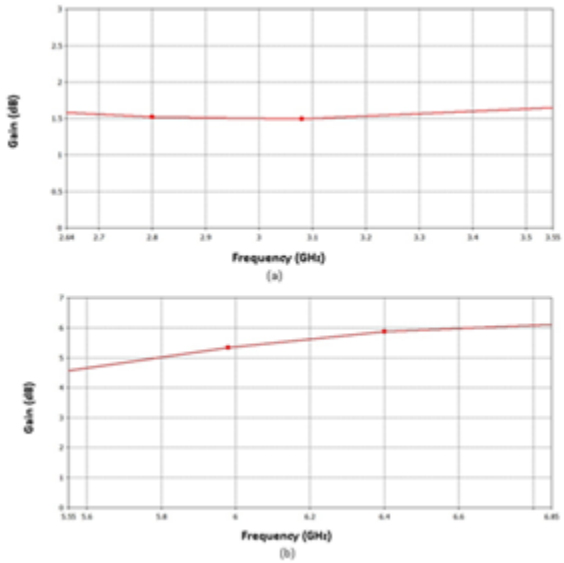

Figure-12. Simulated peak gain of the resulting square printed monopole dual-band antenna at (a) lower resonating band, and (b) upper resonating band

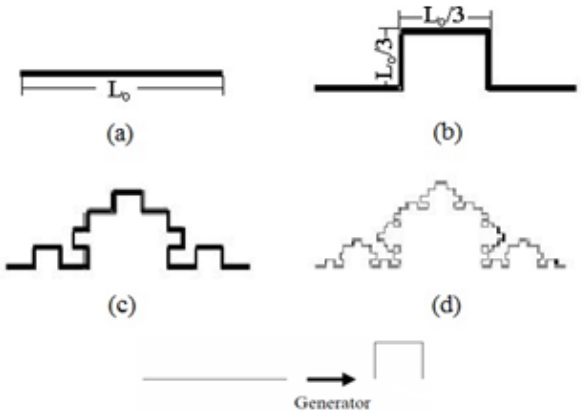

Figure-13. The generation process of the Minkowski space-filling fractal structure; (a) the initiator, (b) the 1st iteration, (c) the 2nd iteration, and (d) the 3rd iteration

5. THE RESULTING ANTENNA DESIGN

The Minkowski space-filling fractal geometry of 1st, 2nd, and 3rd iteration has been used to improve the resonance of the resulting dual-band antenna. Figure 13 shows the generation process of the Minkowski space-filling fractal structure that will be applied to the resulting antenna structure.

The straight line in Figure 13(a) called the initiator is as Euclidean line. The middle third of the initiator will be replaced by the generator, which each segment of it is having a length equal to third the length of the initiator, as shown at the bottom of Figure 13. Each of the five straight segments of the generating structure, shown in Figure 13(b), is replaced with the generator, and so on. This iterative generating procedure continues for an infinite number of times. The final result is a curve with an infinitely intricate underlying structure that is not differentiable at any point.

Figure 9 and Equations (5, and 6) imply that the internal slot length (Ls) and the external length (Lp) of the radiator have a direct effect on the lower resonant frequency. The fractal structure is inserted into the internal slot length (Ls) to increase the electrical current path at the regions between the internal length and external length at both sides of the radiator.

Figure 14 shows the structure of the resulting square printed monopole dual band antenna as taken from the environment of the Computer Simulation Technique (CST) after applying the Minkowski space-filling fractal for; (a) the first iteration, (b) the second iteration, and (c) the third iteration to both the internal slot lengths (Ls1 and Ls2). The center of the modeled antenna is located at the point (0, 0, 0) with respect to the local coordinate system (x, y, z). While its width is in the direction of the x-axis, its length is in the direction of the y-axis, and its thickness is in the direction of the z-axis.

Because the Minkowski space-filling fractal structure is applied to the internal length of both sides of the radiator in the resulting dual band antenna as shown in

Figure 14, therefore the internal length only would be affected, and all external dimensions of the antenna remained at the same values.

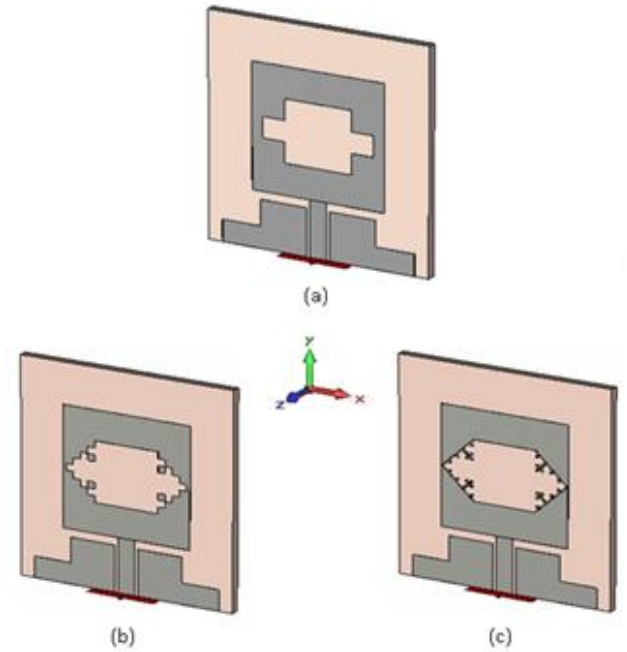

Figure-14. The proposed fractal shaped square ring dual-band antenna with respect to the local coordinate system for; (a) the 1st iteration, (b) the 2nd iteration, and (c) the 3rd iteration

The first iteration consists of 5 segments, and the second iteration has 25 segments, and so on. The length enclosed by any fractal structure at the nth iteration n, Ln is:

$$L_n = L_{n-1} + \frac{\sqrt{L_\circ/3}}{n} \qquad for\ n \geq 1 \qquad (7)$$

where L_{n-1} is the previous internal length (Ls) with the fractal effect. Then the effective length (Leff) would be modified to:

$$L_{eff} = L_n + 0.77L_p \qquad (8)$$

The presence of the irregular radiating edges in the Minkowski space-filling fractal that employed in the antenna structure is a way to increase the surface current path length compared to that of the conventional square slot antenna, resulting in a reduced resonant frequency or a reduction in the antenna size if the design frequency is to be maintained.

The effects of the Minkowski space-filling fractal structure at 1st, 2nd, and 3rd iteration on the input reflection coefficient of the resulting square printed Monopole dual-band antenna is shown in Figure 15. Figure 15 shows the input reflection coefficient response of the four resulting antennas in a swept frequency range from 1 to 10 GHz. In this frequency range, the resulting dual-band monopole antenna, without fractal structure, exhibits a lower resonant band from (2.64 – 3.55) GHz covers 2.5/3.5 GHz WiMAX, and upper resonant band from (5.55 – 6.85) GHz includes 5.8 GHz WLAN.

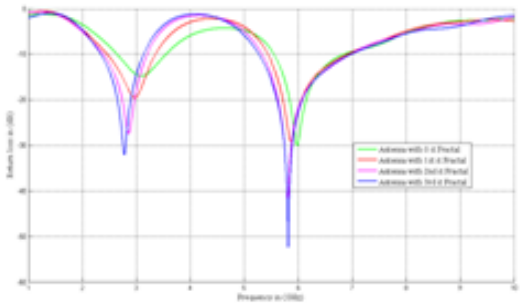

Figure-15. Effects of the Minkowski space-filling fractal structure at 1st, 2nd, and 3rd iteration on the input reflection coefficient of the resulting square printed monopole dual-band antenna

In the resulting square printed monopole dual-band antenna with 1st iteration Minkowski space-filling fractal structure for (S11 ≤ -10 dB), the lower resonant band from (2.46 – 3.36) GHz covers 2.5 GHz WiMAX, and the upper resonant band from (5.44 – 6.92) GHz covers 5.5 GHz WiMAX and 5.8 GHz WLAN.

As for the resulting square printed monopole dual-band antenna with 2nd iteration Minkowski space-filling fractal structure for (S11 ≤ -10 dB), the lower resonant band from (2.39 – 3.2) GHz covers 2.5 WiMAX, (2.4 – 2.484) GHz WLAN, (2.4 – 2.484) GHz Bluetooth, (2.4 – 2.484) GHz ISM, and 2.45 GHz RFID and the upper resonant band from (5.33 – 6.97) GHz covers 5.5 GHz WiMAX and 5.8 GHz WLAN.

On the other hand, the resulting square printed monopole dual-band antenna with 3rd iteration Minkowski space-filling fractal structure for (S11 ≤ -10 dB), the lower resonant band from (2.35 – 3.13) GHz, and the upper resonant band from (5.27 – 6.97) GHz. That means the two bands of this antenna cover all WiFi applications for lower and upper WLAN, 2.5/5.5 GHz WiMAX, (2.4 – 2.484) GHz Bluetooth, (2.4 – 2.484) GHz ISM, and 2.45 GHz RFID.

6. CONCLUSIONS

The extraction of dual-band resonant behavior from the UWB response, using a modification process with the aid of the analysis of the current distribution on the surface of the UWB antenna, has been successfully carried out in this paper. Also, the radiating element of this antenna has been further modified by applying the fractal geometry to improve the resonance of a dual-band response. The input reflection coefficient (S_{11}) responses of the presented antennas reveal the dual-band behavior, which makes all of them suitable for wireless communication applications. In spite of the compact size, the designed antenna demonstrates an average gain, close to omnidirectional radiation pattern throughout the two obtained bandwidths.

The authors hope to extend the application of the proposed technique, in this paper, to extract the dual-band and multiband printed and microstrip antenna responses from the UWB ones when the dimensions of the antenna structures are required to be maintained.

REFERENCES

[1] S. Behera and K. J. Vinoy. 2009. Microstrip square ring antenna for dual-band operation. Progress In Electromagnetics Research, PIER 93, 41-56.

[2] N. Behdad and K. Sarabandi. 2006. A varactor-tuned dual-band slot antenna. IEEE Transactions on Antennas and Propagation, Vol. 54, No. 2, 401-408.

[3] M. A. Alkanhal and A. F. Sheta. 2007. A novel dual-band reconfigurable square-ring microstrip antenna. Prog. In Electromag. Res., PIER 70, 337-349.

[4] A. P. Mishra, P. Singh, N. P. Yadav and J. A. Ansari. 2009. Compact shorted microstrip patch antenna for dual band operation. Progress In Electromagnetics Research, PIER C, Vol. 9, 171-182.

[5] A. Ramadan, M. Al-Husseini, Y. Tawky, K. Y. Kabalan, and A. El-Hajj. 2010. A novel frequency/ pattern-reconfigurable microstrip antenna for WLAN applications. Proceedings of the 4th European Conference on Antenna and Propagation, EuCAP,

[6] Hu, W., Y. Z. Yin, X. Yang, and X. S. Ren. 2010. Compact printed antenna with h shaped stub for dual-band operation. Electronic Lett., Vol. 46, No. 25.

[7] J. R. Panda and R. S. Kshetrimayum. 2011. A printed 2.4 GHz / 5.8 GHz dual-band monopole antenna with a protruding stub in the ground plane for WLAN and RFID applications. Prog. In Electromag. Res., Vol. 117, 425-434.

[8] W.-C. Liu. 2007. Optimal design of dual-band CPW-fed G-shaped monopole antenna for WLAN application. Prog. In Electromag. Res., PIER 74, 21-38.

[9] D. D. Krishna, M. Gopikrishna, C. K. Aanandan, P. Mohanan, and K. Vasudevan. 2008. Compact dual band slot loaded circular microstrip antenna with a superstrate. Progress In Electromagnetics Research, PIER 83, 245-255.

[10] W. Hu, Y. -Z. Yin, S. -T. Fan, J. -Y. Deng, and M. Zhang. 2011. Compact CPW-fed square slot antenna for dual-band operation. Prog. In Electromag. Res., Vol. 20, 165-173.

[11] Y. Zhuo, L. Yan, X. Zhao, and K. Huang. 2011. A compact dual-band patch antenna for WLAN applications. Prog. In Electromag. Res., Vol. 26, 153-160.

[12] C. -J. Wang, Y. -J. Lee, and K. -C. Lee. 2011. A dual-band CPW-fed L-slot Antenna with both linear and circular polarizations. Progress In Electromagnetics Research, PIER C, Vol. 21, 229-241.

[13] Z. Aijaz and S. C. Shrivastava. 2008. Aperture coupled microstrip slot antenna," IEEE International Conference on Recent Advances in Microwave Theory and Applications, Microwave 2008, Jaipur, India.

[14] J. Ghalibafan and A. R. Attari. 2010. A new dual-band microstrip antenna with U-shaped slot. Prog. In Electromag. Res. C, PIER C, Vol. 12, 215-223.

[15] J.K. Ali. 2011. A new dual band e-shaped slot antenna design for wireless applications. Prog. In Electromag. Res. Symposium Proceedings, Suzhou, China, Sept. 12-16.

[16] J.A. Ansari, P. Singh, and S. K. Dubey. 2008. H-shaped stacked patch antenna for dual band operation. Prog. In Electromag. Res. B, PIER B, Vol. 5, 291-302.

[17] S. Gai, Y.-C. Jiao, Y.-B. Yang, C.-Y. Li and J.-G. Gong. 2010. Design of a novel microstrip-fed dual-band slot antenna for WLAN applications. Progress In Electromagnetics Research, Vol. 13, 75-81.

[18] L. Kang, Y. -Z. Yin, H. Li, W. -J. Huang, and S. -F. Zheng. 2010. Dual-wideband symmetrical g-shaped slotted monopole antenna for WLAN/ WiMAX applications. Progress In Electromagnetics Research, Vol. 17, 55-65.

[19] J.K. Ali. 2008. A new miniaturized fractal bandpass filter based on dual-mode microstrip square ring resonator. Proceedings of the 5th International Multi-Conference on Signals, Systems, and Devices, IEEE SSD '08, Amman, Jordan.

[20] J.K. Ali and Y. S. Miz'el. 2009. A new miniature Peano fractal-based bandpass filter design with 2nd harmonic suppression 3rd IEEE International Symposium on Microwave, Antenna, Propagation and EMC Technologies for Wireless Communications, Beijing, China.

[21] J.K. Ali and N. N. Hussain. 2011. An extra reduced size dual-mode bandpass filter for wireless communication systems. Proceedings of Progress in Electromagnetics Research Symposium, PIERS 2011, Suzhou, China.

[22] J.K. Ali, H. Alsaedi, M. F. Hasan and H. A. Hammas. 2012. A Peano fractal-based dual-mode microstrip bandpass filters for wireless communication systems.

Proceedings of Progress in Electromagnetics Research Symposium, PIERS 2012, Moscow, Russia.

[23] J.K. Ali and H. Alsaedi. 2012. Second harmonic reduction of miniaturized dual-mode microstrip bandpass filters using fractal shaped open stub resonators. Progress in Electromagnetics Research Symposium, PIERS 2012, KL, Malaysia.

[24] J.K. Ali, N.N. Hussain, A.J. Salim, H. Alsaedi. 2012. A new tunable dual-mode bandpass filter design based on fractally slotted microstrip patch resonator. Progress in Electromagnetics Research Symposium. pp. 1225-1228.

[25] Y.S. Mezaal, H.T. Eyyuboglu, J.K. Ali. 2013. A novel design of two loosely coupled bandpass filters based on Hilbert-zz resonator with higher harmonic suppression. Proc. IEEE 3rd International Conference on Advanced Computing and Communication Technologies, (ACCT). pp. 343-347.

[26] Y.S. Mezaal, H.T. Eyyuboglu and J.K. Ali. 2013. New dual band dual-mode microstrip patch bandpass filter designs based on Sierpinski fractal geometry. IEEE Third International Conference on Advanced Computing and Communication Technologies, ACCT, pp. 348-352, Rohtak, India.

[27] Y.S. Mezaal, H.T. Eyyuboglu, and J.K. Ali. 2014. Wide bandpass and narrow bandstop microstrip filters based on Hilbert fractal geometry: design and simulation results. PloS one. 9: 1-12.

[28] Y.S. Mezaal, H.T. Eyyuboglu and J.K. Ali. 2014. New microstrip bandpass filter designs based on stepped impedance Hilbert fractal resonators. IETE Journal of Research. 60(3): 257-264.

[29] Y.S. Mezaal, J.K. Ali and H.T. Eyyuboglu. 2015. Miniaturised microstrip bandpass filters based on Moore fractal geometry. International Journal of Electronics. 102(8): 1306-1319.

[30] J.K. Ali and H.T. Ziboon. 2016. Design of compact bandpass filters based on fractal defected ground structure (DGS) resonators. Indian Journal of Science and Technology. 9: 1-9.

[31] Ahmed, H.S., Salim, A.J., Ali, J.K., Alqaisy, M.A. 2017. A fractal-based dual-mode microstrip bandstop filter for wireless applications Mediterranean Microwave Symposium.

[32] H.S. Ahmed, A.J. Salim, M.R. Hussan, H.A. Hammas, M.T. Yassen, S. Mutashar, J.K. Ali. 2018. Design of compact dual-mode fractal based microstrip band reject filter. ARPN Journal of Engineering and Applied Sciences. 13(7): 2395- 2399.

[33] Y.S. Mezaal, H.T. Eyyuboglu and J.K. Ali. 2013. A new design of dual band microstrip bandpass filter based on Peano fractal geometry: Design and simulation results. 13th IEEE Mediterranean Microwave Symposium, MMS'2013, Saida, Lebanon.

[34] M.A. Alqaisy, Ali, J.K., Chakrabarty, C.K., Hock, G.C. 2013. Design of a compact dual-mode dual-band microstrip bandpass filter based on semi-fractal CSRR. Progress in Electromagnetics Research Symposium.

[35] H.S. Ahmed, A.J. Salim, and J.K. Ali. 2015. A Compact dual-band bandstop filter based on fractal microstrip resonators. Progress in Electromagnetics Research Symposium, PIERS 2015, Prague, Czech Republic.

[36] M. Alqaisy, C. Chakrabraty, J.K. Ali and A.R. Alhawari. 2015. A miniature fractal-based dual-mode dual-band microstrip bandpass filter design. International Journal of Microwave and Wireless Technologies. 7(2): 127-133.

[37] H.S. Ahmed, A.J. Salim, J.K. Ali and N.N. Hussain. 2016. A compact triple band BSF design based on Minkowski fractal geometry. Proceedings of 18th IEEE Mediterranean Electrotechnical Conference, MELECON 2016, Limassol, Cyprus.

[38] H.T. Ziboon and J.K. Ali. 2017. Compact quad-band BPF design with fractal stepped-impedance ring resonator. ARPN Journal of Engineering and Applied Sciences. 12(24): 7352-7363.

[39] H.T. Ziboon and J.K. Ali. 2017. Compact dual-band bandpass filter based on fractal stub-loaded resonator. Progress in Electromagnetics Research Symposium, St Petersburg, Russian Federation.

[40] H.T. Ziboon and J.K. Ali. 2018. Design of a triple-band fractal-based BPF with asymmetrical SLR structures. Journal of Engineering and Applied Sciences. 13(7), pp.1617-1620.

[41] J.K. Ali, Z.A.A. AL-Hussain, A.A. Osman, and A.J. Salim. 2012. A new compact size fractal based microstrip slot antenna for GPS applications. Proceedings of Progress in Electromagnetics Research Symposium, PIERS, pp. 700-703, Kuala Lumpur, Malaysia.

[42] J.K. Ali, A.J. Salim, A.I. Hammoodi, and H. Alsaedi. 2012. An ultra-wideband printed monopole antenna

with a fractal based reduced ground plane. Proceedings of Progress in Electromagnetics Research Symposium. Moscow, Russia.

[43] J.K. Ali and E.S. Ahmed. 2012. A new fractal based printed slot antenna for dual band wireless communication applications. Proceedings of Progress in Electromagnetics Research Symposium, PIERS, pp. 1518-1521, Kuala Lumpur, Malaysia.

[44] Ali, J., Abdulkareem, S., Hammoodi, A., Salim, A., Yassen, M., Hussan, M. and Al-Rizzo, H., 2016. Cantor fractal-based printed slot antenna for dual-band wireless applications. International Journal of Microwave and Wireless Technologies, 8(2), pp.263-270.

[45] S.F. Abdulkarim, A.J. Salim, J.K. Ali, A.I. Hammoodi, M.T. Yassen and M.R. Hassan. 2013. A compact Peano-type fractal based printed slot antenna for dual-band wireless applications. Proceedings of IEEE International RF and Microwave Conference, RFM, pp. 329-332, Penang, Malaysia.

[46] J.K. Ali, M.T. Yassen, M.R. Hussan, and A.J. Salim. 2012. A printed fractal based slot antenna for multi-band wireless communication applications. In Proceedings of Progress in Electromagnetics Research Symposium, Moscow, Russia.

[47] J.K. Ali. 2009. A new microstrip-fed printed slot antenna based on Moore space-filling geometry. IEEE Loughborough Antennas and Propagation Conference, LAPC 2009, Loughborough, U.K, pp. 449-452.

[48] P. Tilanthe, P. C. Sharma, and T. K. Bandopadhyay. 2011. A compact UWB antenna with dual band rejection. Progress In Electromagnetics Research, PIER B, Vol. 35, 389-405.